Environ Geochem Health
https://doi.org/10.1007/s10653-023-01718-1

ORIGINAL PAPER

Sulfidic schist release of As, Cu, and Pb in laboratory experiments and across eleven watersheds in central Massachusetts, USA

Justin B. Richardson · Stephanie A. Thrasher · Brian Saccardi · Elyse V. Clark

Received: 23 January 2023 / Accepted: 28 July 2023

Abstract Sulfidic schists are important rock formations due to their trace metal and metalloid (TMM) content and carry the potential for pyrite and pyrrhotite to hydrate and oxidize leading to acid-enhanced chemical weathering. The objectives of this study were to compare TMMs in sulfidic schists to other co-occurring bedrock, evaluate conditions that optimize TMM rock weathering, and examine streamwater TMMs in relation to bedrock lithology and human development in eleven streams across central Massachusetts. Sulfidic schists samples had the highest As (72 ± 46 mg kg^{-1}), Cu (63 ± 21 mg kg^{-1}), and Pb (63 ± 33 mg kg^{-1}) concentrations. Electron Probe Microanalysis (EPMA) images show As and Pb were widely distributed across silicate and sulfide minerals in both the mica schist and sulfidic schists, not exclusively hosted in sulfide minerals as hypothesized. Batch reactors had TMM dissolution rates an order of magnitude higher for sulfidic schists than granite and mica schists. Furthermore, TMM dissolution was greatest under pH 9 than pH 7 or pH 5 and dissolution rates were two times greater under anoxic conditions compared to oxic conditions. Streamwater concentrations of As (0.01 to 10.3 µg L^{-1}), Cu (0.2 to 206 µg L^{-1}), and Pb (0.001 to 8.3 µg L^{-1}) were below Massachusetts Surface Water Quality Standards. Across the eleven watersheds, % sulfidic schists were positively correlated with mean streamwater S and Cu concentrations and area-normalized annual export. Streamwater As and Pb concentrations were significantly correlated with %Developed land and %Mica schist, which strongly covaried. Our study confirmed the elevated abundance of TMMs in sulfidic schists but laboratory experiments suggest the precipitation of amorphous Fe oxyhydroxide phases decreased dissolved TMMs during oxic weathering. Future work will need to incorporate groundwater and stable isotope systems to separate anthropogenic and geogenic analyses.

Keywords Trace metals and metalloids · Streamwater · Batch reactor · Sulfide weathering

Supplementary Information The online version contains supplementary material available at https://doi.org/10.1007/s10653-023-01718-1.

J. B. Richardson (✉) · S. A. Thrasher · B. Saccardi
Department of Geoscience, University of Massachusetts Amherst, 233 Morrill Science Center, Amherst, MA 01003, USA
e-mail: jbrichardson@umass.edu

J. B. Richardson
School of Earth and Sustainability, University of Massachusetts Amherst, Amherst, MA 01003, USA

E. V. Clark
Department of Earth and Geographic Sciences, Fitchburg State University, Fitchburg, MA 01420, USA

Published online: 11 August 2023

Introduction

An important group of metamorphic rocks are sulfidic schists, which are metamorphosed sediments containing the iron sulfide minerals pyrite and pyrrhotite. It is thought that the sulfidic schist protoliths are formed as sediments, or possibly in the diagenetic phase and contain between 0.3 and >3% sulfur (S) by mass (Tracy & Robinson, 1988, Parnell, 1982). Sulfidic schists are important for several economic and environmental reasons. Economically, they can serve as hosts for ores and metal sources. As examples, sulfidic schists in Talvaivaara, Finland, are used as polymetallic ores (Pakostova et al., 2017) and magmatic deposits used as a nickel (Ni) ore in Kabanga, Tanzania (Evans et al., 2000). Environmentally, sulfidic schists can negatively impact surface and groundwater resources. The pyrite and pyrrhotite within sulfidic schists can hydrate and oxidize when exposed to water seeping through rock fractures (Pye & Miller, 1990; Mahoney et al., 2019; Gu et al., 2020). This oxidation process can release trace metals and metalloids (TMMs) substituted within pyrite and pyrrhotite and from accessory minerals such as galena, chalcopyrite, and arsenopyrite (e.g., Koski et al., 2008; Zhu et al., 2008; Perkins & Mason, 2015; Richardson et al., 2018). Furthermore, the oxidation of sulfide minerals can be through abiotic oxidation-hydration processes or through microbially mediated process and lead to the formation of SO_3^{-2}, SO_4^{-2}, or other oxyhydrated S forms (e.g., Evangelou & Zhang, 1995; Percak-Dennett et al., 2017). One of the most important chemical weathering products from pyrite and pyrrhotite is the production of H_2SO_4 which can accelerate rock chemical weathering (Evangelou & Zhang, 1995) and the solubility of TMMs released from sulfide minerals. However, the oxidation of Fe^{+2} to Fe^{+3} and resulting precipitation of Fe oxyhydroxides can adsorb and immobilize the released TMMs (Pye & Miller, 1990; Mahoney et al., 2019). In addition, Fe released from Fe-bearing aluminosilicates in schists such as biotite can also lead to Fe oxyhydroxide formation (Aldridge & Churchman, 1991). Thus, sulfidic schists serve as important TMM hosts with the internal mechanisms for feedback cycles for TMM sequestration or mobilization.

Arsenic (As), copper (Cu), and lead (Pb) are three important TMMs present in groundwater and surface waters throughout New England and other regions globally. Naturally sourced As and Pb negatively impact groundwater with potential hazards to human health. Santangelo et al. (2022) found elevated Pb in private wells across Massachusetts exceeding EPA primary drinking water standards and Ayotte et al. (2003) finding elevated As in public groundwater supplies across New England well-over the EPA primary drinking water standard. Since watersheds are integrators of geologic, biologic, and anthropogenic activities, the presence of TMM-rich sulfidic schists in a watershed may cause groundwater surface water quality degradation that may otherwise be attributed to human activities. Oxidation of galena and arsenopyrite have been long hypothesized as the dominant sources of As and Pb across southern New England (Ayotte et al., 2003; Kim et al., 2002), with suspected impacts on groundwater and surface waters at the watershed scale. Arsenic and Pb can act as potent carcinogen and neurotoxin, respectively, with severe impacts on children chronically exposed to elevated concentrations in drinking water (Ayotte et al., 2003; Mohod et al., 2013). In particular, the oxidation and release of Cu from chalcopyrite may negatively impact aquatic ecosystems. Algae, invertebrates, amphibians, and fish are sensitive to Cu toxicity (Azizishirazi et al., 2021; Eisler, 1998). For example, Brook trout (*Salvelinus fontinalis*) is an important species ecologically and for recreational fishing but has been reduced or greatly reduced in Massachusetts rivers (Eastern Brook Trout Joint Venture, 2006). This decline has been attributed to physical barriers fragmenting rivers and decreases in water quality due to sediments, temperature, oxygen content, and contaminants (Eastern Brook Trout Joint Venture, 2006; Sotiropoulos et al., 2006).

However, linking surface water quality with specific geologic deposits and geochemical processes can be difficult due to anthropogenic overprinting. In addition to geologic sources, there are many potential anthropogenic sources of As, Cu, and Pb at the watershed scale in central Massachusetts, including modern car brakes particulates, industrial activities, historical fuel combustion, legacy mill dam sediments, pesticides, and smelting (Ozdilek, 2002; Richardson et al., 2015). Thus, human-derived TMMs co-occur with the geogenic-driven biogeochemistry of TMMs within watersheds.

In our study, we focused on nested watersheds spanning a range of urban densities and abundance

of sulfidic schists within central Massachusetts to investigate impacts on surface water quality. The objectives of this study were to (1) determine the concentrations and minerals hosting As, Pb, and Cu in sulfidic schists and other co-occurring dominant bedrock (2) evaluate the conditions that optimize TMM weathering release from bedrock samples, and (3) examine differences in streamwater TMMs in relation to bedrock lithology and human developments to evaluate geogenic vs. anthropogenic watershed scale effects. For objective (1) and (2), we expected to find higher TMM concentrations and dissolution rates in sulfidic schists than other local rock types, demonstrating their importance as a TMM source to surface waters and groundwaters. Moreover, we expected highest dissolution rates under oxic, acidic solutions comparable to soil or near surface regolith conditions. However, inherited or neoformed Fe oxyhydroxide may act as a sink for TMMs derived from weathering, limiting TMM release under oxic conditions. For objective (3), we expect the underlying sulfidic schist bedrock to significantly increase dissolved TMMs in streamwater samples compared to other bedrock lithologies. However, we also expect that Cu and Pb will be enriched in watersheds with extensive human development and watersheds with wetlands to sequester As, Cu, and Pb. Quantifying the retention or release of TMMs from sulfidic schists is needed to determine the importance of sulfide weathering on water quality as well as terrestrial TMM biogeochemical cycling.

Materials and methods

Study area—central Massachusetts

We conducted the study in central Massachusetts, which contains the Merrimack Synclinorium and Bronson Hill Anticlinorium and has a mix of igneous and metamorphic bedrocks. Deformation in the Bronson Hill Anticlinorium was caused by the end of the Taconic orogeny when the Bronson Hill Arc collided with Laurentia. The Acadian orogeny caused deformation in the Merrimack synclinorium (Robinson et al., 1982). Sulfidic schists comprise the Silurian Paxton Formation (Walsh, 2002) and the Middle-Ordovician Partridge Formation (Parnell, 1982). The Partridge Formation are metamorphosed black shale mantling gneiss domes. The composition and weathering of the sulfidic schists of the Partridge Formation, a two-mica feldspar schist with graphite and pyrrhotite, was well-characterized in Parnell (1982). Here, we are focused on the Paxton Formation, a sillimanite–muscovite–plagioclase–quartz schist containing pyrrhotite and local abundances of black tourmaline (Walsh, 2002). Similar to the Partridge Formation, the Paxton Formation is believed to be the result of metamorphosed black shale and volcanic sediments. Igneous intrusions, forming sills of granite and pegmatites intruding within the Paxton and Littleton Formation are known as the Fitchburg plutons (Walsh, 2002). The granites and pegmatites are syntectonic intrusive bodies parallel with the regional foliation resulting from the Acadian orogeny (Robinson & Goldsmith, 1991).

Overall, the climate of the watershed consists of mild to hot summers with no dry season, with coldest month averaging below 0 °C. Annual precipitation averages > 1100 mm, and the region is classified as humid continental (Dfa) using the Köppen climate classification. Forests are predominantly northern hardwoods: maples (*Acer* spp.), American beech (*Fagus grandifolia*), oak (*Quercus* spp.), birch (*Betula* spp.), and interspersed poplars (*Populus* spp.), ash (*Fraxinus* spp.) and basswood (*Tilia Americana*). Areas with steep slopes, shallow soils, and bouldery areas are predominantly pine (*Pinus* spp.) and eastern hemlock (*Tsuga canadensis*). The surface geology and derived-soils are dominated by shallow, rocky glacial till in local uplands ranging in 1 to 3 m depth with outwash, lacustrine, and fluvial materials present in concave lowlands. Most soils are skeletal-loamy sand deposits derived from glacial till to well-sorted silty loam deposits of glaciofluvial materials in riparian floodplains.

We studied eleven nested watersheds within the North Nashua River or adjacent within the larger Nashua River watershed of central Massachusetts (Fig. 1). W3 and W4 are in the Nashua River watershed but not the North Nashua River watershed. W5 through W10 are nested within the North Nashua River watershed, which is W11. W1 and W2 are also in the North Nashua River watershed, but drain into the main river channel downstream of W11. The Nashua River watershed is ideal for studying the effect of sulfidic schists processes at the watershed scale due to the abundance of sulfidic schists

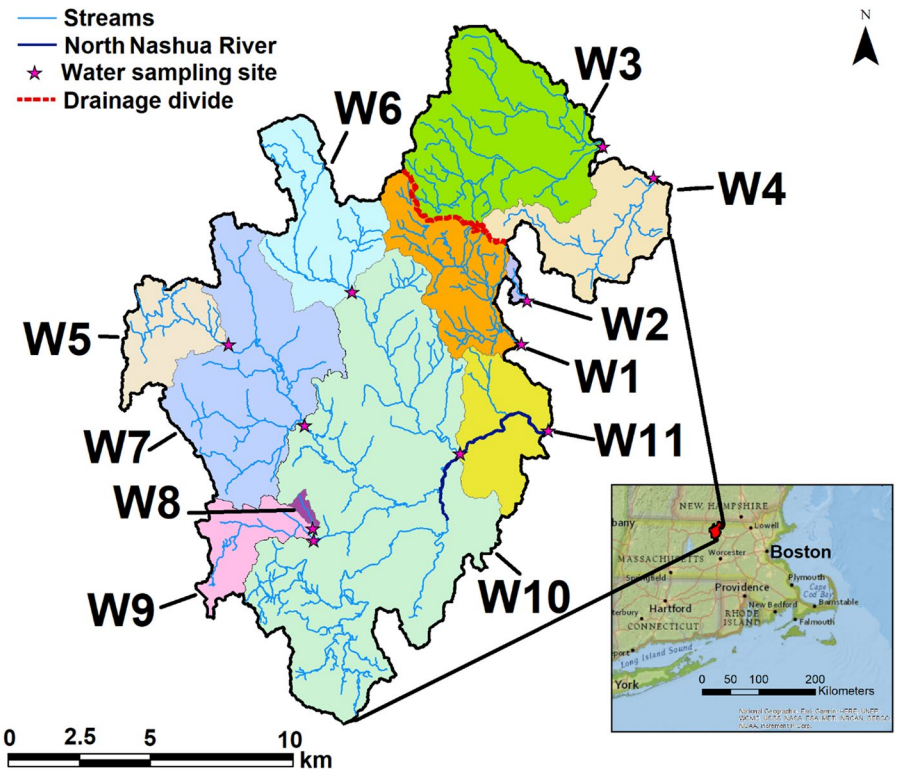

Fig. 1 A map displaying the site location of the watersheds in central Massachusetts. Bottom right inset map shows the watersheds with respect to Boston and southern New England. Right map shows the eleven adjacent or nested watersheds studied streamlines, the mainstem of the North Nashua River, and the drainage divide between the North Nashua and the Nashua River watersheds

intermixed with other rock types to evaluate impacts while keeping regional upland-hilly topography and peri-urban anthropogenic effects comparable. The watersheds range in size from 1.1 km^2 up to 303.4 km^2 and geologic composition from 1 to 100% sulfidic schist, 0 to 99% granite, and 0 to 64% mica schist bedrock based upon USGS Massachusetts bedrock geology map (Table 1). Moreover, the watersheds ranged from 5 to 26% developed land (sum of open space, low-, medium-, and high- intensity developed land) 48 to 85% forested, 4 to 11% wetland, and 1 to 9% agricultural land (sum of pasture/hay and cultivated crops) based upon NLCD 2019 data (Table 1; Fig. 2; Dewitz & USGS, 2021).

Description of rock, soil, and streamwater sampling

Twenty-two rock samples were collected from the four most common types of bedrock within the watersheds, which were granites, granofels, mica schists, and sulfidic schists (Fig. 2). Lithologic, surface deposit, and topographic maps were used to identify road cuts, river cuts, steep hillslopes, and shallow regolith areas that might contain accessible outcrops and shallow bedrock for sampling. To collect suitable rock samples with limited weathering, a rock hammer or rock pry bar was used to safely expose new faces. The latitude and longitude coordinates of each sample were recorded. Bedrock samples were dried in a convection oven at 70 °C for 72 h. For imaging, 2- to 4-cm chips were made for mineralogical and elemental imaging. For elemental analyses and chemical weathering experiments, bedrock samples were ground with a tungstate mill and passed through a 100-mesh sieve (< 150 µm).

Streamwater sampling of the eleven watersheds was designed to capture seasonal patterns but not intensive enough to capture individual storm events. Streamwater samples were collected biweekly between February 2020 to November 2020 and monthly December 2020 to September 2021. Streamwater samples were collected as handheld dip samples in the center of the channel using 500-mL acid-washed polyethylene bottles. Sampling locations were in wadable straight channel reaches with relatively uniform flow. Water samples were filtered to < 0.2 µm and measured for pH and electrical conductivity (EC) using Atlas Scientific probes in the laboratory.

Table 1 Description of stream names, and watershed areas

	Watershed	Watershed area	%Sulfidic Schist	%Granite	%Mica schist	%Granofel	%Dev	%Forest	%Wetland	%Agri
		km^2	%	%	%	%	%	%	%	%
W1	Scott Brook	28.2	1	99	0	0	5	80	4	6
W2	Fitchburg High Tributary	1.2	1	99	0	0	5	83	8	4
W3	Willard Brook	60.6	2	94	3	1	8	75	7	8
W4	Pearl Hill Brook	28.6	1	69	11	18	5	85	6	1
W5	Whitman River-Ashburnham	18.5	100	0	0	0	7	70	11	3
W6	Phillips Brook	31.9	30	43	27	0	8	75	7	5
W7	Whitman River	82.4	67	12	21	0	10	70	10	5
W8	Town Farm Rd Tributary	1.1	34	2	64	0	15	69	7	9
W9	Old Town Farm Rd Tributary	14.6	18	7	52	23	26	48	19	4
W10	Nashua River North	278.8	17	35	48	0	14	67	8	6
W11	Nashua River Downtown	303.4	17	36	49	0	18	65	7	5

Bedrock lithology of Massachusetts is from US Geological Survey (USGS) based upon mapping by Zen et al. (1983). Land use data is from NLDC (2018). %Dev. is the sum of open, light, medium, and high intensity human development and %Agri. is the sum of sum of pasture/hay and cultivated crops area using NLCD 2019 (Dewitz & USGS, 2021)

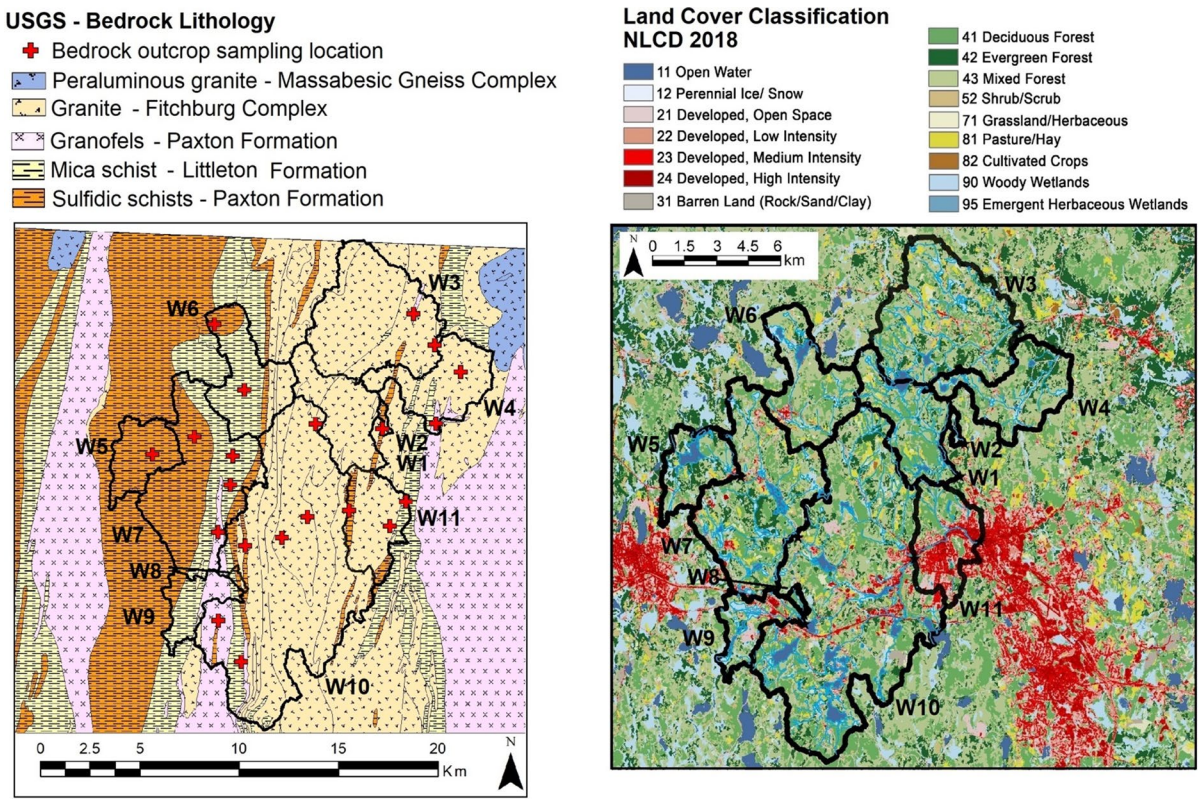

Fig. 2 Left map shows USGS bedrock lithology map based upon mapping by Zen et al. (1983) with respect to the eleven watersheds. Right map shows land cover classification data from NLCD (2018) across the eleven watersheds

The 500 mL samples were then dried down to 50 g sample in an open vessel in a fume hood with 5 mL of 30% H_2O_2 to remove organic matter, and 5 mL of 70% HNO_3 to keep metals dissolved. Preparation blanks were also performed to quantify and assess contamination.

Rock analyses

Total rock digestions using nitric acid (HNO_3) and hydrofluoric acid (HF) were completed in order to fully break down. Three replicates of 50 ± 5 mg of each rock sample were measured into 15-mL Teflon vials and sealed with 2.5 mL of HNO_3 and 2.5 mL HF. The samples were boiled on a hot plate for 72 h at 180 °C. Once there were no visible solids, the vials were unsealed and the samples were allowed to dry down at 100 °C without fully drying out. When the samples achieved gel-like consistency 1.5 mL of HNO3 was added and repeated three times. In the final step, 3 mL of HNO3 and deionized (DI) water were added to each vial. The vials were resealed and boiled at 100 °C for 24 h. After this process was completed, the samples were carefully transferred to 50-mL centrifuge tubes and DI water was added to bring the final digestate volume to 25 mL. Every 20 samples included two USGS rock standards (SDC-1 and GSP-2) and a digestion blank. Once the digestions were completed, the samples were analyzed for macroelements with an Agilent 5110 ICP-OES and TMMs with an Agilent $7700 \times$ ICP-MS. Concentrations in the preparation blank were < 0.01 mg L^{-1} for macroelements and < 0.1 ug L^{-1} for TMMs and all rock sample process-digestion duplicates were within 15% coefficient of variation (CV). Recovery for macroelements and TMMs in USGS SDC-1 and GSP-2 were 83 to 104% of their certified values.

Total concentrations of S in rocks were determined using a X-200 XRF instrument from SciAps (SciAps Inc., Woburn, MA), and concentrations of Al, Fe, Ca,

K were also checked using XRF. For each rock sample, 10 g of crushed sample were packed into 7-mL polypropylene vessels lined with polyethylene terephthalate sheet. The X-200 utilizes three energy beams: 40 kV, 10 kV, and 50 kV, from an Rh anode alloy. For a detector, it uses a 20-mm 2-silicon drift detector and 135 eV resolution FWHM at 5.95Mn K-alpha line. Spectra were analyzed using Compton Normalization (EPA Method 6200). To account for inaccuracies in the software, data were further processed with a multi-element regression model developed from nine USGS rock standards (the additional four were BHVO-2, DNC-2, BIR-1, BCR- 2, SBC-2, SDO-1, SDC-1, STM-2, GSP-2, W-2a). Total Al, Fe, Ca, K, and S concentrations were within 16% of their certified values, and duplicates were within 6% relative standard deviation.

Batch reactors

Batch reactors were completed to understand how the three most common bedrock types (sulfidic schist, granite, and mica schist) release TMMs under different aqueous conditions mimicking acidic, oxic conditions in forested shallow glacial till to alkaline, anoxic confined aquifers. We have focused only on granite, mica schists and sulfidic schists due to granofel TMM concentrations being comparable or lower than granite. Following methods described in Richardson et al. (2022), 5.00 ± 0.10 g of each bedrock powder was measured into 50-mL centrifuge tubes in triplicate. Eight total treatments were used to assess the effect of pH and oxic conditions, which is important as groundwater can be reducing with a pH ~ 8 where as soils and near surface regolith can be exposed to oxic, acidic conditions. To create the pH treatment solutions, we used diluted pH buffer modified with diluted trace metal grade sodium hydroxide (NaOH) or nitric acid (HNO_3) used for pH standards. The treatments were pH 5, pH 7, and pH 9. Ambient conditions present in the dilute buffer solutions were oxic conditions with approximately 240 mV at pH 9, 280 mV at pH 7 and 310 mV at pH 5 throughout the experiment. To create the reducing treatment, solutions were reduced with 0.002 M sodium dithionite to achieve approximately −250 mV based upon Fe reduction analyses by Mehra and Jackson (2013). For each reactor, 40 mL of solution for each treatment was added to the bedrock powders and shaken with an Eberbach table-top reciprocating shaker at 180 oscillations per minute. Every third day, solutions were removed from the shaker, centrifuged at 2500 rpm for 45 min and 0.2 mL was removed and diluted to 15 mL, then acidified to pH 1 with 0.2 g of 15 M HNO_3 to determine the change in macroelement and TMM concentrations over the course of fifteen days. The pH was measured and adjusted with HNO_3 or NaOH while oxic/reducing conditions did not deviate from their original values. Diluted extracts were analyzed for macroelements with an Agilent 5110 ICP-OES and TMMs with an Agilent 7700 × ICP-MS. The change in mean concentrations of the triplicates were plotted with time and the slope of the linear regression model was used as the weathering rate.

The surface areas of crushed rock samples used in batch reactors (sulfidic schist, granite, mica schist) were analyzed by Brunauer–Emmett–Teller (BET) method commercially by Particle Testing Authority following ASTM C1069-09 (ASTM 2014). In brief, samples were oven-dried and degassed to purge vapors under N_2 for 960 min at 25 °C. Surface area was calculated using a seven-point calibration curve of saturation pressure (ranging from 80 to 120 kPa) and temperature (75.4 to 78.9 K).

Scanning electron microscope, energy-dispersive X-ray spectroscopy, and X-ray diffraction

Three rock chips, approximately 1 cm × 1 cm, derived from the granite, mica schist, and sulfidic schist samples were fixed in epoxy resin, cut to expose the unweathered surface, coated in carbon and imaged at University of Massachusetts Amherst Electron Microprobe/ SEM Facilities. First, rock chips were imaged by using a scanning electron microscope (SEM) and energy-dispersive X-ray spectroscopy (EDS) to identify mineral assemblages and potential trace metal-bearing phases. EDS was also used to obtain quantitative data on mineral compositions and conducted with a beam current of 200.0 nA and voltage of 15 kV on a Zeiss Evo 50 SEM. Next, the samples were imaged by electron probe microanalysis (EPMA) using a Cameca SX five wavelength-dispersive X-ray spectroscopy (WDS) for As, Cu, and Pb.

Mineralogy of the crushed rock samples was determined by X-ray diffraction (XRD). Crushed rock subsamples were washed with DI water and dried three times to remove ultrafine particles and

were mineralogy confirmed by XRD patterns measured. For quantification of mineral abundances, 0.5 g of each sample was mounted on a glass slide and analyzed between 5 and 55° 2θ (0.02° resolution, 1° min^{-1}) using a Rigaku Miniflex-2 (Rigaku Analytical Devices, Wilmington, MA, USA) equipped with a Cu Kα X-ray source. Quantification was performed using the Rietveld whole pattern profile fit module in PDXL2.

Discharge rates and watershed export estimations

Streamwater discharge for the North Nashua River at W11 was determined using data from the USGS NWIS system, as it is gauged at USGS site 01094400 in Fitchburg, MA. However, discharge from the USGS is not available for the ten other watersheds, as they are substantially smaller watersheds. To estimate stream discharge, a yearly discharge data from ten additional USGS gauged rivers in central Massachusetts and eastern Connecticut were used (See Supplemental Information for specific watersheds and estimates). The watershed area (A) and discharge rates (D) were logarithmically transformed, then plotted and fitted with a straight, linear line to determine the scaling parameters (b for the intercept; m for the slope) per Eq. (1). The R^2 of the regression was 0.87 with the slope $m = 1.2327$ and intercept $b = 193{,}663$.

$$D = bA^m \tag{1}$$

Using Eq. (1), the annual discharge for the ten watersheds was estimated (Supplemental Fig. 1; Supplemental Table 1). To estimate monthly watershed export, the proportion of the monthly discharge from north Nashua River between Dec 1, 2019, and Oct 31, 2021. Average monthly concentrations were multiplied by the average monthly discharge and summed to determine an annual flux mass for each element (e.g., Richardson, 2020). For months where multiple water samples were collected the median concentration was used. While not ideal due to missing stochastic discharge events which cause large fluxes (e.g., tropical storms, spring snowmelt) and variability in subsurface and surface water storage (e.g., shallow uplands, wetland storage, deeper fluvial deposits), the data set provides for an estimate of elemental export and normalization for differences in watershed area.

Statistical analyses

Descriptive statistics as well as parametric and nonparametric statistical tests were calculated in MATLAB (Mathworks, Natick, MA, USA). In text values either report minimum and maximum values; arithmetic mean values ± 1 standard error (SE) are presented in text and in figures. Variability in data was assessed using relative standard deviation (RSD), calculated as the difference within the same sample. Since sample sizes were small and did not meet criteria to be parametric, the nonparametric Kruskal–Wallis test was used for comparisons among three or more samples, and post hoc Wilcoxon signed rank tests were used to compare differences among rock fragments, batch reactor dissolution rates, and dissolved trace element concentrations among watersheds. To examine relationships at the watershed-scale among streamwater pH, dissolved elements, bedrock rock, and watershed land-use properties, data were tested for normality, logarithmically transformed (log base 10) when necessary, and compared with Pearson linear regressions.

Results

Bulk rock chemistry and SEM imaging

There were wide ranges and some significant differences in bulk rock macroelements and TMMs across the rock types. The granofel had significantly lower Al but significantly higher Ca than the granite and mica schist ($p < 0.05$; Supplemental Fig. 3; Table 2). The sulfidic schist did not have significantly different macroelement chemistry than any other rock type, except having higher S concentrations by a factor of 100× ($p < 0.01$). For TMMs, granofels had significantly lower As than the other rock types ($p < 0.05$). Sulfidic schists had significantly higher As, Cu, and Pb than the other three rock types ($p < 0.05$).

From SEM images and EDS (Supplemental Fig. 2) and XRD (Table 2), we observed similar mineralogy present in granite, mica schist, and sulfidic schist samples with abundant quartz, albite, and micas. However, the mica schist also contained 6% ferrosilite and the sulfidic schists contain 12% pyrrhotite, existing as elongated bands. The EPMA images were used

Table 2 Mean macro- and trace element concentrations in unweathered bedrock samples

	N	Al	Fe	Ca	K	Mg	Na	S	P
		%	%	%	%	%	%	%	μg g^{-1}
Granite	6	8.8 ± 0.5	3.1 ± 2.9	0.8 ± 0.4	3.3 ± 0.7	0.6 ± 0.4	1.3 ± 0.7	0.01 ± 0.00	760 ± 250
Granofel	4	6.7 ± 0.4	4.3 ± 0.4	1.5 ± 0.3	2.2 ± 0.1	1.6 ± 0.5	1.9 ± 0.6	0.01 ± 0.00	584 ± 33
Mica schist	5	8.9 ± 1.8	4.2 ± 1.0	0.8 ± 0.6	2.4 ± 1.3	1.3 ± 0.7	0.6 ± 0.4	0.02 ± 0.00	601 ± 196
Sulfidic schist	7	8.1 ± 2.1	5.9 ± 3.1	1.4 ± 1.2	3.2 ± 2.2	1.0 ± 0.7	1.0 ± 0.3	1.23 ± 0.84	586 ± 202
	N	As	Cr	Co	Cu	Mn	Ni	Pb	Zn
		μg g^{-1}	μg g^{-1}	μg g^{-1}	μg g^{-1}	μg g^{-1}	μg g^{-1}	μg g^{-1}	μg g^{-1}
Granite	6	19 ± 12	36 ± 18	36 ± 15	16 ± 7	450 ± 180	11 ± 4	30 ± 14	84 ± 42
Granofel	4	9 ± 2	1 ± 1	102 ± 44	13 ± 3	389 ± 112	49 ± 22	34 ± 4	94 ± 7
Mica schist	5	33 ± 17	145 ± 58	161 ± 64	27 ± 14	772 ± 323	34 ± 25	21 ± 9	151 ± 34
Sulfidic schist	7	72 ± 46	123 ± 144	131 ± 74	63 ± 21	774 ± 278	54 ± 31	63 ± 33	157 ± 23
	N	Surface area	Quartz	Albite	Mica	Pyrrhotite	Chlorite	Ferrosilite	Calcite
		m^2/g	%	%	%	%	%		%
Granofel	3	0.422	36	26	32	–	–		4
Mica schist	3	2.089	35	13	38	< 2	4	6	< 2
Sulfidic schist	3	3.934	35	9	44	12	–		–
Granite	3	0.314	49	34	15	< 2	–		–

Error shown is ± 1 standard deviation

to qualitatively evaluate if TMMs are hosted within sulfide minerals or within other phases. Here, we are using Al abundance as a proxy for aluminosilicate minerals and Fe abundance as a proxy for sulfide and overlapping Al–Fe as Fe bearing-aluminosilicate minerals. The EPMA images (Fig. 3) suggest that As and Pb are widely distributed across minerals in both the mica schist and sulfidic schist rocks and not exclusively hosted in sulfide minerals as hypothesized. However, Cu was more clearly associated with some Fe phases for the mica schist. Similarly, Cu was more associated with Fe phases than As and Pb were associated with Fe phases in the sulfidic schist. There is high background noise for As, Cu, and Pb due to elevated concentrations in rare earth element concentrations in monazite through the mica schist and sulfidic schist samples.

Batch reactors

We utilized batch reactors for three major rock types under varying pH and oxic conditions to evaluate aqueous conditions driving TMM release during rock chemical weathering. Linear regression models for each rock and element had slopes ranging 1 to 2 orders of magnitude in rate (Table 3) with R^2 values of 0.6 to 0.9 and p values were < 0.01, except for low concentrations for granite S and Pb and mica schist Pb which had p values < 0.05 but R^2 values of only 0.3. Generally, we observed significantly higher Fe, As, Cu, and Pb release rates under pH 9 compared to pH 7 and pH 5 and observed many significantly higher release rates under anoxic than oxic conditions using the Kruskal–Wallis test with post hoc Wilcoxon signed rank test. Aluminum release rate was highest for mica schist under pH 9 conditions ($p < 0.05$, Table 3). Sulfidic schists had higher Fe release rates than granite and mica schists under all conditions. Interestingly, Fe release rates were significantly higher under pH 9 than pH 7 or pH 5 across the three rock types. Sulfur release rates were significantly higher for mica schist than granite ($p < 0.05$). Further, S release was significantly higher for sulfidic schists than mica schists by a factor of ~ 10 × and higher than granite by a factor of > 100 × ($p < 0.01$). Unfortunately, since sulfides were used as the reducing agent in the experiment, anoxic S release could not be quantified. For TMMs, As, Cu and Pb release rates were significantly higher for sulfidic schists than granite and mica schists by at least an order of magnitude. Sulfidic schist TMM release was greatest under pH 9 than pH 7 and 5 by a factor of 2 or 3 in most

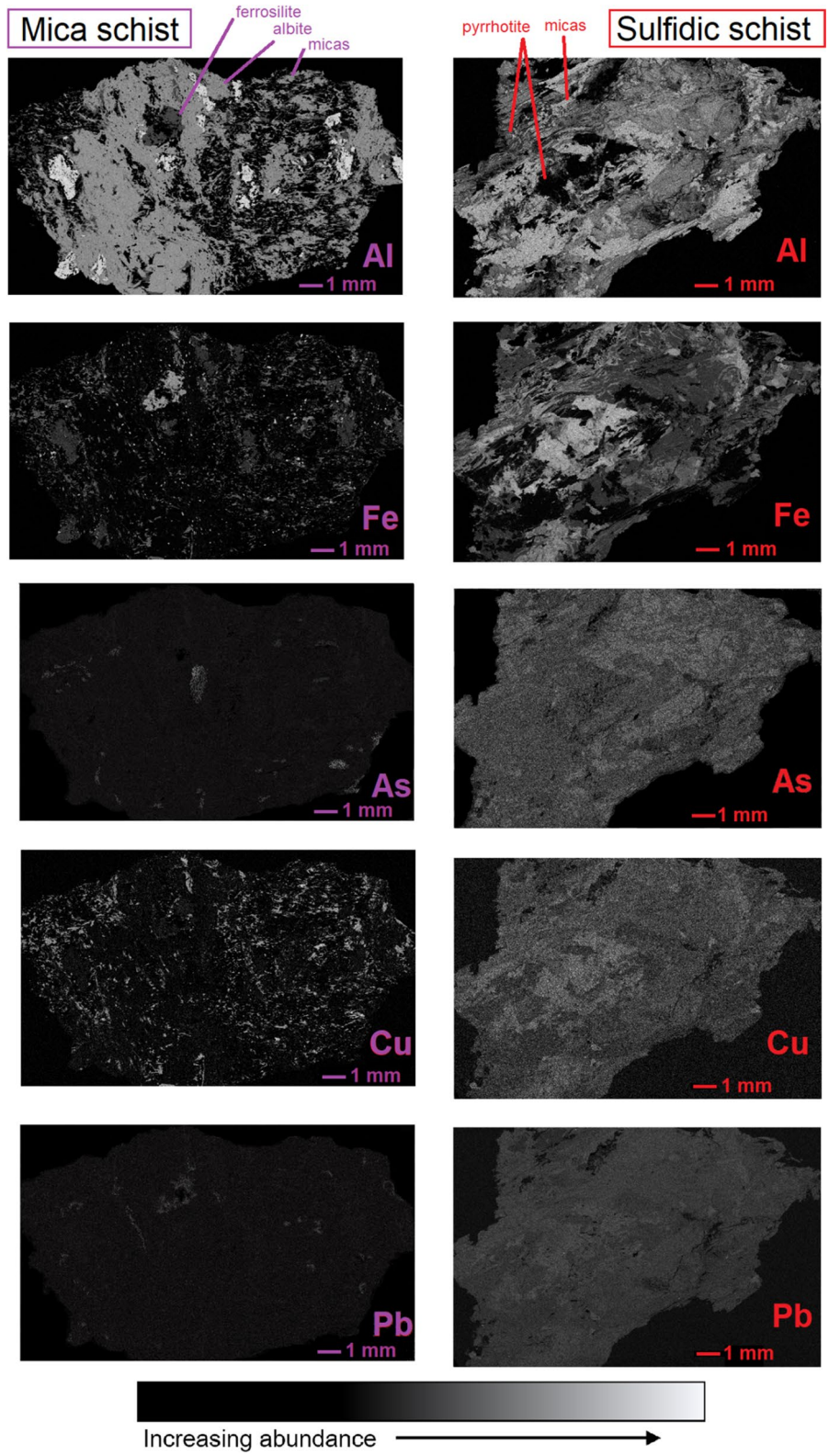

Fig. 3 EPMA images of rock samples, with the left column of mica schist and right column of sulfidic schists

Table 3 Batch reactor rock weathering rate slopes

		Al		Fe		S		As		Cu		Pb	
		Oxic	Anoxic	Oxic	Anoxic	Oxic	Anoxic	Oxic	Anoxic	Oxic	Anoxic	Oxic	Anoxic
		mg d^{-1} m^{-2}	mg d^{-1} m^{-2}	mg d^{-1} m^{-2}	mg d^{-1} m^{-2}	mg d^{-1} m^{-2}	mg d^{-1} m^{-2}	mg d^{-1} m^{-2}	mg d^{-1} m^{-2}	mg d^{-1} m^{-2}	mg d^{-1} m^{-2}	mg d^{-1} m^{-2}	mg d^{-1} m^{-2}
Granite	pH 9	1.6 ± 0.4	1.1 ± 0.5	49 ± 10	81 ± 11	0.2 ± 0.0	N/a	0.5 ± 0.2	1.1 ± 0.4	0.5 ± 0.2	2.2 ± 1.0	0.2 ± 0.0	0.5 ± 0.0
	pH 7	1.1 ± 0.4	0.5 ± 0.2	43 ± 9	55 ± 10	0.5 ± 0.1	N/a	1.1 ± 0.5	1.6 ± 0.3	0.5 ± 0.2	2.2 ± 0.8	0.2 ± 0.0	0.2 ± 0.0
	pH 5	2.2 ± 0.4	2.7 ± 1.1	9 ± 3	46 ± 6	0.2 ± 0.0	N/a	1.1 ± 0.4	2.2 ± 1.1	1.1 ± 0.3	1.6 ± 0.7	0.2 ± 0.0	0.2 ± 0.0
Sulfidic schist	pH 9	1.1 ± 0.3	0.5 ± 0.3	181 ± 39	278 ± 91	19 ± 6	N/a	19 ± 5	39 ± 13	21 ± 9	42 ± 13	19 ± 6	39 ± 16
	pH 7	0.1 ± 0.1	0.1 ± 0.2	6 ± 2	19 ± 7	0.6 ± 0.3	N/a	0.6 ± 0.2	1.4 ± 1.4	0.6 ± 0.2	3.3 ± 1.4	0.6 ± 0.2	1.7 ± 0.8
	pH 5	0.1 ± 0.1	0.1 ± 0.2	4 ± 1	15 ± 5	0.5 ± 0.2	N/a	0.6 ± 0.2	0.9 ± 1.2	0.6 ± 0.3	2.9 ± 1.2	0.6 ± 0.1	1.5 ± 0.6
Mica schist	pH 9	0.1 ± 0.1	0.3 ± 0.1	1 ± 1	1 ± 0	0.1 ± 0.0	N/a	0.1 ± 0.1	0.2 ± 0.1	0.2 ± 0.1	0.2 ± 0.1	0.1 ± 0.0	0.1 ± 0.0
	pH 7	0.3 ± 0.1	0.3 ± 0.1	1 ± 1	1 ± 0	0.1 ± 0.0	N/a	0.2 ± 0.1	0.3 ± 0.0	0.1 ± 0.0	0.1 ± 0.0	0.1 ± 0.0	0.1 ± 0.0
	pH 5	0.4 ± 0.1	0.4 ± 0.1	1 ± 0	1 ± 0	0.2 ± 0.0	N/a	0.3 ± 0.1	0.3 ± 0.0	0.1 ± 0.0	0.1 ± 0.0	0.1 ± 0.0	0.1 ± 0.0

Batch reactor experiments were conducted in triplicate over 15 days of weathering. Every 3 days, 0.1 mL of solution was collected to determine the change in dissolved Al, S, Fe, As, Cu, and Pb. A linear regression was fit to the mean of the triplicate data and the slopes and error of the slopes are presented in this table. Error shown is ± 1 standard deviation of the triplicate. N/A indicates data not available due to S being part of dithionite used to generate reducing conditions

cases. Moreover, sulfidic schist TMM release was 2 × greater on average in anoxic conditions compared to oxic conditions.

Streamwater concentrations and export

While many watersheds had similar streamwater chemistry, there were some significant differences. Streamwater pH was largely comparable across all watersheds except in W2 which was significantly lower than all other watersheds except W8 (Fig. 4, Supplemental Table 2). Streamwater Fe and Si were not significantly different among the watersheds. Streamwater S and As were significantly lower for W1, W2, W3, and W4 than W8, W9, and W10. Streamwater Cu was significantly higher for W2, W 4, and W7 than the other watersheds. Lastly, streamwater Pb was significantly higher for W7, W9, and W11 than W1, W3, W5, and W8.

Watershed export rates of macroelements and TMMs for the eleven watersheds were determined using the measured river water concentrations and actual discharge rates between Dec 1, 2019, and Oct 31, 2021 (see Sect. "Discharge rates and watershed export estimations"). Unsurprisingly, the watersheds with the largest areas had the highest discharge totals. Watersheds 10 and 11 had the highest total export rates for all macroelements and TMMs, with export rates 1–2 magnitudes higher than other watersheds in some cases (Table 4). Watershed 7 had higher total export rates than all other watersheds for S, As, Cu, and Pb. When macroelement and TMM export rates were normalized per unit area of the watershed, W10 and W11 still had some of the highest area-normalized export rates for all elements analyzed, whereas W5 and W8 had the lowest area-normalized export rates (Table 4). However, W11 had much higher area normalized Pb export than W10.

Streamwater linkages with watershed lithology and human development

Using linear regressions to compare stream concentrations and area-normalized watershed export with bedrock and lithology, we found several significant trends. Across the eleven watersheds, mean streamwater Fe, S, and As concentrations were negatively correlated with %Granite but positively correlated with %Mica schist (Table 5). Further, mean streamwater S and Cu were positively correlated with %Sulfidic schist. Comparing area-normalized annual export with watershed lithology, we observed %Sulfidic schist was positively correlated with Fe, S, and Cu and %Mica schist was positively correlated with As and Cu. %Granofels was present at only two watersheds and was not significantly correlated with any concentration or area-normalized export.

Considering human developments, mean streamwater Fe, As, and Pb concentrations were positively correlated with %Developed, especially As with $R > 0.8$. Conversely, mean streamwater Fe, As, and Pb concentrations were negatively correlated with %Forest. Mean streamwater Fe and Pb concentrations were positively correlated with %Wetland. Comparing area-normalized annual export with land development, some trends were lost. Area-normalized export of Cu was positively correlated with %Developed while conversely area-normalized export of Fe and Cu was negatively correlated with %Forest. %Wetland was not correlated with any element but %Agricultural was negatively correlated with Fe and Pb. Unfortunately, %Developed and %Mica schist coverage of the eleven watersheds covaried and were significantly correlated with each other with an R^2 value of 0.83.

Discussion

Elevated TMMs and rock weathering rates by sulfidic schists

In our first hypothesis, we expected that sulfidic schists would host higher TMM concentrations and generate higher TMM release rates that other local bedrocks within pyrrhotite and other sulfide minerals. Our results support that sulfidic schist samples had higher As, Cu, and Pb concentrations than mica schists, granofels, and granite within the central Massachusetts region. This agrees with other previous studies that found elevated TMMs in sulfide-bearing sedimentary and metamorphic rocks (Parnell, 1982; Koski et al., 2008). However, our results show that As, Cu, and Pb concentrations were only a factor of 2 higher than mica schists and a factor of 2 to 3 times higher than granite concentrations. Furthermore, there was high variability for As (minimum and maximum of 5 to 271 mg kg^{-1}), Cu

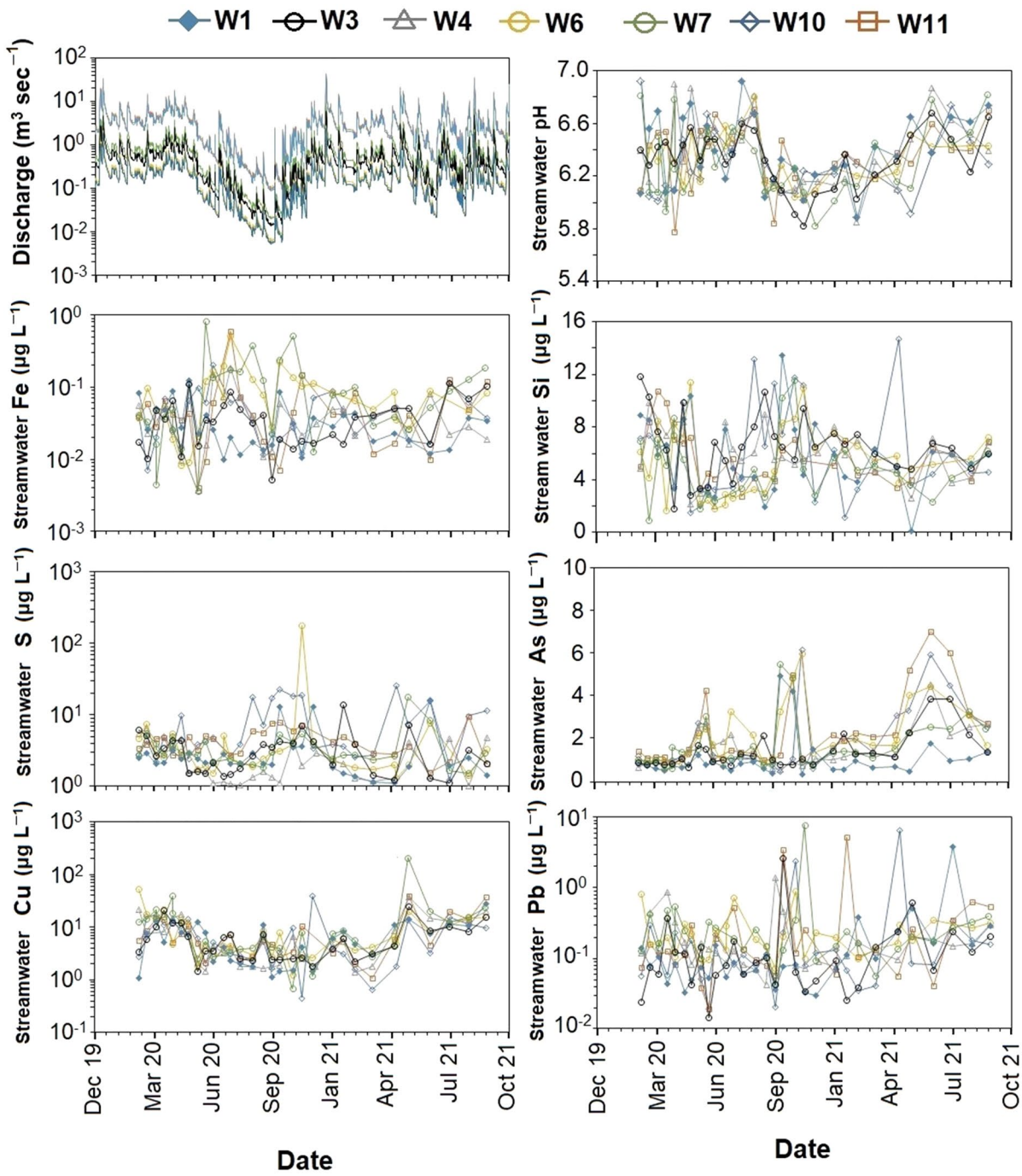

Fig. 4 Stream discharge, pH, and TMM concentrations for seven of the eleven watersheds which were constant throughout the monitoring period. W2, W5, W8, and W9 were not plotted due to their intermittent flow during summers

(12 to 231 mg kg^{-1}), and Pb (57 to 158 mg kg^{-1}) concentrations with relative standard deviation of over ~ 50%. This wide variability is likely due to differences in protolith, diagenetic processes, and quartz content (Parnell, 1982; Tracy & Robinson, 1988).

Table 4 Estimated total export rates and area-normalized export rates for the eleven watersheds studied

	Discharge $m^3\ yr^{-1}$	Al Mg yr^{-1}	Fe Mg yr^{-1}	Si Mg yr^{-1}	S Mg yr^{-1}	As kg yr^{-1}	Cu kg yr^{-1}	Pb kg yr^{-1}
W1	10^7	0.29	0.25	35	24	4.5	35.0	0.4
W2	10^5	0.007	0.005	0.6	0.4	0.1	2.0	0.03
W3	10^7	0.70	0.43	91	60	13.4	94.8	1.6
W4	10^7	0.30	0.23	35	17	5.8	42.1	1.4
W5	10^6	0.13	0.32	13	11	3.2	38.7	0.7
W6	10^7	0.28	0.44	40	72	9.1	65.5	1.5
W7	10^7	1.57	1.14	98	70	23.4	194.8	11.3
W8	10^5	0.004	0.004	0.7	0.8	0.2	1.0	0.0
W9	10^6	0.12	0.24	17	10	3.8	17.0	3.9
W10	10^8	2.70	4.49	458	470	120.7	1276.6	13.1
W11	10^8	4.51	6.45	664	419	150.7	711.2	95.9
	Watershed area	Al	Fe	Si	S	As	Cu	Pb
	km^2	Mg $yr^{-1}\ km^{-2}$	Mg $yr^{-1}\ km^{-2}$	Mg $yr^{-1}\ km^{-2}$	Mg $yr^{-1}\ km^{-2}$	kg $yr^{-1}\ km^{-2}$	kg $yr^{-1}\ km^{-2}$	kg $yr^{-1}\ km^{-2}$
W1	28.2	0.010	0.009	1.2	0.9	0.16	1.2	0.01
W2	1.2	0.006	0.004	0.5	0.3	0.06	1.6	0.02
W3	60.6	0.012	0.007	1.5	1	0.22	1.6	0.03
W4	28.6	0.011	0.008	1.2	0.6	0.20	1.5	0.05
W5	18.5	0.007	0.027	0.7	1.6	0.17	2.1	0.04
W6	31.9	0.009	0.014	1.3	1.2	0.29	2.1	0.05
W7	82.4	0.019	0.014	1.2	0.8	0.28	2.4	0.14
W8	1.1	0.004	0.004	0.6	0.7	0.14	0.9	0.01
W9	14.6	0.008	0.016	1.2	0.7	0.26	1.2	0.27
W10	278.8	0.010	0.016	1.6	0.7	0.43	4.6	0.05
W11	303.4	0.015	0.021	2.2	1.4	0.50	2.3	0.32

Export rates are based upon monthly concentrations and monthly discharge rates, either measured by USGS or estimated from regional USGS measurements (see methodology description in Sect. "Discharge rates and watershed export estimations")

We further expected TMMs to be predominately held within sulfide minerals but our results suggest mixed origins. Using Al as a proxy for aluminosilicates and Fe as a proxy for sulfide and Fe bearing aluminosilicates, our EPMA maps suggest TMMs were distributed across multiple phases but Cu and Pb appear more concentrated in sulfide phases. The accumulation of TMMs within the sulfide phases matches previous observations. However, the wide distribution of As in aluminosilicate phases was unexpected, and may be due to background noise from small monazite phases, high Al or Si concentrations, or potential substitution of As into the silicates (Alam et al., 2014).

Lastly, our batch reactor experiment compared the release rates of TMMs from granite, granofel, mica schist, and sulfidic schists and their results show that sulfidic schists released As, Cu, and Pb generally an order of magnitude faster than the other rocks. Although the sulfidic schist TMM concentrations were less than an order of magnitude higher than the granofels, mica schists, and granite, their higher TMMs release rates demonstrate that sulfides were more susceptible to chemical weathering than silicate minerals. These results agree with previous evaluations that suggest sulfide phases can have higher rock weathering rates (Parnell, 1982, Koski et al., 2008). In addition, the results agree with previous studies that found that chemical weathering of silicates can release TMMs, potentially those substituted within silicate minerals such as biotite (Masuda et al., 2012). Furthermore, we observed that reducing conditions had higher Fe, As, Cu, and Pb release rates, which

Table 5 R values for linear regressions for watershed bedrock and land-use properties with macroelement and TMM river water concentrations and area-normalized annual export rates. Bold *R* values are significant at $p < 0.05$

Streamwater	%Sulfidic schist	%Granite	%Mica schist	%Granofel	%Developed	%Forest	%Wetland	%Agri
pH	0.2	−0.1	−0.2	0.1	−0.1	−0.1	−0.1	−0.3
Al	**−0.5**	0.1	0.3	0.4	0.1	0.1	−0.2	0.2
Fe	0.3	**−0.6**	**0.5**	0.4	**0.6**	**−0.7**	**0.8**	−0.1
Si	0.2	−0.4	0.3	0.1	0.3	−0.3	0.3	0.3
S	**0.5**	**−0.5**	**0.6**	−0.3	0.3	−0.3	0.0	0.3
As	−0.1	**−0.6**	**0.9**	0.3	**0.8**	**−0.7**	0.3	0.2
Cu	**0.5**	−0.1	−0.3	−0.3	−0.3	0.2	0.1	−0.2
Pb	0.0	−0.3	**0.5**	0.3	**0.7**	**−0.7**	**0.5**	−0.1
Area-normalized export	%Sulfidic schist	%Granite	%Mica schist	%Granofel	%Developed	%Forest	%Wetland	%Agri
Al	0.1	0.0	−0.1	−0.1	0.0	0.0	−0.1	−0.1
Fe	**0.7**	**−0.6**	0.1	0.0	0.3	**−0.5**	0.4	**−0.5**
Si	−0.3	0.1	0.3	0.0	0.3	−0.3	−0.1	0.1
S	**0.6**	−0.3	−0.1	−0.3	0.0	−0.2	0.0	0.0
As	−0.3	0.1	**0.5**	0.0	0.3	−0.3	−0.1	0.1
Cu	**0.5**	**−0.6**	**0.5**	−0.1	**0.5**	**−0.5**	0.2	−0.3
Pb	0.3	0.0	−0.2	−0.1	−0.3	0.2	0.2	**−0.5**

was converse to our hypothesized mechanism of sulfide oxidation leading to TMM release. The higher release of As, Cu, and Pb under basic, reducing conditions suggests that deep groundwater is likely a more important zone for TMM release than shallow groundwater. In a study of nearby watersheds in central Massachusetts by Yuretich et al. (1989), shallow, high velocity flow paths generated acidic, oxic groundwater while deeper, slower flow paths yielded circumneutral, reduced groundwater. Based upon the importance of flow paths and velocities, groundwater undergoing deeper, slower flow paths generating circumneutral and low oxygen conditions may be an important driver of TMM release to surface waters.

As described by Parnell (1982), the hydration and oxidation driving dissolution of sulfides requires oxygen additions to the system, resulting in releases of Fe, which undergoes rapid oxidation of Fe^{+2} to Fe^{+3}. We hypothesize that the dissolution of sulfides under oxic conditions in the batch reactors may have been higher than under reducing conditions; however, the oxic conditions allowed for formation of amorphous Fe oxyhydroxide phases that adsorbed or precipitated TMMs from solution (e.g., Koski et al., 2008; Perkins & Mason, 2015; Qiu et al., 2018). This agrees with findings by Pye and Miller (1990), Koski et al. (2008) and Mahoney et al. (2019) in which Fe is not mobile during pyrite and sulfide oxidative weathering. Additionally, we found that basic conditions of pH 9 had higher release rates of Fe and TMMs than acidic conditions of pH 5. This was also converse to our expected proton promoted dissolution of sulfides. We hypothesize that the either the basic conditions allowed for less TMM adsorption on Fe oxyhydroxides formed during rock weathering or the acidic conditions released higher amounts of Fe and TMMs which were precipitated or adsorbed and thus not measured. As shown by Koski et al. (2008), high pH solutions can have comparable dissolution of TMMs from sulfide-bearing rocks but the abundance of Fe oxyhydroxides can alter the dissolved phases. However, the dissolution of sulfides under basic conditions are generally considered to be limited but our results suggest this may simply prevent secondary Fe oxyhydroxide from adsorbing TMMs, which may not be universally the case. For example, hydroxylation of pyrite and other sulfides may be an important and understudied mechanism for dissolution (e.g., Cohn et al., 2004; Xian et al., 2019). Thus, our batch reactors provide insight on the generation of soluble TMMs but not necessarily the full picture on mechanisms promoting their solubility.

Streamwater linked with sulfidic schist, mica schist, and human development

Our third objective was to utilize a set of nested subwatersheds to examine if bedrock lithology and human developments generated watershed scale effects of elevated TMM concentrations in streamwaters. The variation in streamwater macroelements, TMMs, and pH across the eleven watersheds had few significant differences. Mean streamwater pH was comparable and concentrations of macroelements and TMMs were all within a factor of 3. Mean streamwater Fe, As, Cu, and Pb concentrations in this study were higher than found in a previous study of the Deerfield subwatersheds in western Massachusetts and Thames River subwatersheds of eastern Connecticut (Richardson, 2020) (minimum mean and maximum mean were Fe: 0.01 to 0.03 mg L^{-1}, As: 0.1 to 0.5 µg L^{-1}, Cu: 1 to 3 µg L^{-1}, and Pb: 0.1 to 0.2 µg L^{-1}). Moreover, the Deerfield and Thames River subwatersheds had lower area normalized exports of Fe (0.001 to 0.002 Mg yr^{-1} km^{-2}) and As (0.04 to 0.31 kg yr^{-1} km^{-2}) but comparable area normalized exports of Cu (0.1 to 2.1 kg yr^{-1} km^{-2}) and Pb (0.01 to 0.18 kg yr^{-1} km^{-2}). Importantly, streamwater concentrations of As, Cu, and Pb were below the Criterion Maximum Concentration and Criterion Continuous Concentrations set by Massachusetts Surface Water Quality Standards, 314 Code of Massachusetts Regulations (CMR) 4.00 and their 2021 amendments. Thus, our results imply limited direct hazards to aquatic life.

Our results suggest that the subwatersheds underlain with sulfidic schists did not have significantly higher As and Pb streamwater concentrations or area-normalized export rates, implying other geochemical and hydrological factors are controlling TMM transport from bedrock to streamwater at the watershed scale. First, colloidal transport which is important for TMMs with low solubility such as Pb may be prevented by sediment trapping dams (e.g., Davidson et al., 2021; Dow et al., 2020; Mierzykowski & Carr, 2000), or As and Cu may become insoluble sulfide forms when buried within wetland and hydric soil sinks (see Baker et al., 1992; Hale et al., 2019). Lastly, hydrologic transport pathways through unconsolidated glaciofluvial materials do not appear favorable for As, Pb, and Cu transport (Roy & Bickerton, 2010; Yellen & Boutt, 2010). For example, the inclusions of carbonate-rich layers within the Paxton formation can increase the pH promoting sorption of trace elements. Further, inclusions of carbonates within the schists can mediate acidity generated by pyrite weathering and drive precipitation of Fe oxyhydroxides increasing adsorption (Nordstrom, 1982; Koski et al., 2008; Huminicki & Rimstidth, 2009; Mahoney et al., 2019). As shown by Yuretich et al (1989), the acid neutralization capacity of crystalline metamorphic bedrock and glacial till in central Massachusetts likely prevents positive-feedback loops enhancing acidification during sulfide oxidation and in streamwater. This is reflected in our streamwater samples being weakly acidic, ranging between pH 6.0 and 6.6 (Fig. 4).

Cole and Boutt (2021) found that ~ 40% of river discharges across shallow glacial till-dominated terrains in Massachusetts are < 3 months in age, showing a strong connection between groundwater and streamwater. During drought conditions in August–September 2020, discharge rates hit their lowest levels and we observed spikes in several elements such as Si, As, Pb, Fe. We hypothesize that lower volume of transport increased TMM concentrations via reverse dilution effect. Thus, TMM concentrations increase with increases in groundwater residence time meaning that equilibrium is not reached under most normal flow conditions. However, there is a possibility that with limited precipitation, discharge became groundwater dominated and elevated As and Pb from groundwater was able to impact surface waters. Without groundwater data, we are unable to provide direct evidence of the later mechanism. These results indicate different types of natural processes may contribute to elevated concentrations of As, Cu, or Pb in the watersheds in this study.

We utilized regressions of bedrock area coverage and land development area to evaluate lithologic and human controls on mean river water concentrations and area-normalized annual export estimates across the eleven watersheds. Our results found some evidence that watersheds with more sulfidic schists had higher mean streamwater concentrations and area normalized export rates for S and Cu. Further, watersheds with more granite had lower macroelement and TMM exports. However, mica schists were most associated with higher mean river water concentrations and area normalized export for macroelements and As and Pb. Anthropogenic effects

also appear important as developed area was also strongly correlated with macroelement as well as As and Pb export. Arsenic and Pb can be related to recent pesticide and municipal sources but may also be related to historic mill pond sediments containing contamination from industrial manufacturing in Fitchburg in the 1800s (e.g., Davidson et al., 2021; Dow et al., 2020; Mierzykowski & Carr, 2000). However, the area of %Developed and %Mica schist of the eleven watersheds covaried and were significantly correlated with each other with an R^2 value of 0.83. From the regressions, we cannot conclude if the abundance of mica schists or human pollution was responsible for higher macroelements and TMMs in river water and watershed exports. Based upon the additional fact that %Forest was negatively correlated with macroelement and As and Pb concentrations, there is additional evidence suggesting the removal of forests for human activity increases the amount of macroelements and TMMs in river water. The negative correlation between %Forest and river water Fe, As, and Pb was observed in Richardson (2020). These results suggest there are some lithologic controls on elements in river water and their area normalized export rates, with sulfidic schists causing higher S and Cu in river water. However, there appears to be a strong effect of land conversion to human developments increasing macroelements as well as As and Pb in streamwater but it cannot be clearly differentiated from mica schists due to the covariance.

Conclusions and future research needs

Our study confirmed the elevated abundance of TMMs in sulfidic schists compared to other bedrocks in the central Massachusetts region. However, there is considerable variability in TMM concentrations (sometimes nearly two orders of magnitude and ~ %50 relative standard deviation) in the sulfidic schists. Thus, there may be small portions of the Paxton formation with outsized effects on surface waters. Laboratory experiment batch reactor data highlight that low oxygen, high pH had the highest TMM release across all three rock types, contrary to the idea of oxic, acidic conditions driving weathering. We suspect the release of Fe and precipitation of amorphous Fe oxyhydroxide phases decreases dissolved TMMs during oxic weathering. Moreover, proton driven dissolution may not be as important as hydroxylation of sulfide minerals.

In our last set of hypotheses, we identified some linkages at the watershed scale between TMMs and bedrock lithology area and land development area. For example, S and Cu were linked with sulfidic schist abundance across the eleven watersheds. Unfortunately, there was a strong covariance between abundance of mica schist and area developed by humans and thus separating the lithologic and anthropogenic effects cannot be clearly understood from this data. We hypothesize that geochemical tools such as stable isotope ratios and pseudo-isotope systems can highlight enrichment of TMMs in streamwater from human activities. Furthermore, we acknowledge an important gap in our study is not characterizing groundwater and subsurface flow. Future work in this area will need to incorporate groundwater to determine if higher concentrations of macroelements and TMMs are found at the bedrock–groundwater interface and how fluxes in groundwater lead to releases of macroelements and TMMs to surface water.

Acknowledgements We thank Ivan Mischenko and Justin Mistikawy for site selection and collection of the rock samples, and Eliza Fitzgerald for helping process the rock samples and conducting some of the digestions. This project was funded by University of Massachusetts Amherst College of Natural Sciences to Dr. Justin Richardson.

Author contributions Dr. Justin B. Richardson led the study conceptualization, methodology, bedrock and soil field sampling, writing of the original draft, visualization of figures and tables, and supervision of the project. Undergraduate researcher Stephanie A. Thrasher contributed to writing, bedrock field sampling, visualization of data. PhD candidate Brian Saccardi contributed to Data analyses and visualization of the watersheds and aided with, review and editing. Dr. Elyse V. Clark contributed to study conceptualization, methodology, field sampling of streamwaters, writing the original draft, and manuscript reviewing and editing.

Funding College of Natural Sciences, University of Massachusetts Amherst, 2018–1001.

Declarations

Competing interests The authors declare no competing interests.

References

Alam, M., Wu, Y., & Cheng, T. (2014). Silicate minerals as a source of arsenic contamination in groundwater. *Water, Air, & Soil Pollution, 225*(11), 1–15.

Aldridge, L. P., & Churchman, G. J. (1991). The role of iron in the weathering of a climosequence of soils derived from schist. *Soil Research, 29*(3), 387–398.

Ayotte, J. D., Montgomery, D. L., Flanagan, S. M., & Robinson, K. W. (2003). Arsenic in groundwater in eastern New England: Occurrence, controls, and human health implications. *Environmental Science & Technology, 37*(10), 2075–2083.

Azizishirazi, A., Klemish, J. L., & Pyle, G. G. (2021). Sensitivity of amphibians to copper. *Environmental Toxicology and Chemistry, 40*(7), 1808–1819.

Baker, L. A. (1992). Introduction to nonpoint source pollution in the United States and prospects for wetland use. *Ecological Engineering, 1*(1–2), 1–26.

Cohn, C. A., Borda, M. J., & Schoonen, M. A. (2004). RNA decomposition by pyrite-induced radicals and possible role of lipids during the emergence of life. *Earth and Planetary Science Letters, 225*(3–4), 271–278.

Cole, A., & Boutt, D. F. (2021). Spatially-resolved integrated precipitation-surface-groundwater water isotope mapping from crowd sourcing: Toward understanding water cycling across a post-glacial landscape. *Frontiers in Water, 3*, 645634.

Davidson, K. B., Holmes, B. E., Spooner, I. S., Dunnington, D. W., Walker, T. R., Lake, C. B., & Su, C. C. (2021). Application of the paleolimnological method to assess metal contaminant distribution (As, Cu, Pb, Zn) in pulp mill stabilization basin sediments, Nova Scotia Canada. *Environmental Science and Pollution Research, 28*(37), 51342–51355.

Dewitz, J., & U.S. Geological Survey. (2021). National land cover database (NLCD) 2019 products (ver. 2.0, June 2021). In U.S. Geological survey data release. https://doi.org/10.5066/P9KZCM54

Dow, S., Snyder, N. P., Ouimet, W. B., Martini, A. M., Yellen, B., Woodruff, J. D., Newton, R. M., Merritts, D. J., & Walter, R. C. (2020). Estimating the timescale of fluvial response to anthropogenic disturbance using two generations of dams on the South River, Massachusetts, USA. *Earth Surface Processes and Landforms, 45*(10), 2380–2393.

Eastern Brook Trout Joint Venture. (2006). Eastern brook trout: Status and threats. Trout unlimited. Available: < http://easternbrooktrout.org/reports/eastern-brook-trout-status-and-threats/view>. Accessed Dec 28 2023.

Eisler, R. (1998). *Copper hazards to fish, wildlife, and invertebrates: A synoptic review (no. 33)*. Reston: US Department of the Interior, US Geological Survey.

Evangelou, V. P., & Zhang, Y. L. (1995). A review: Pyrite oxidation mechanisms and acid mine drainage prevention. *Critical Reviews in Environmental Science and Technology, 25*(2), 141–199.

Evans, D. M., Boadi, I., Byemelwa, L., Gilligan, J., & Marcet, P. (2000). Kabanga magmatic nickel sulphide deposits, Tanzania: Morphology and geochemistry of associated intrusions. *Journal of African Earth Sciences, 30*(3), 651–674.

Gu, X., Heaney, P. J., Reis, F. D. A., & Brantley, S. L. (2020). Deep abiotic weathering of pyrite. *Science, 370*(6515), eabb8092.

Hale, R., Swearer, S. E., Sievers, M., & Coleman, R. (2019). Balancing biodiversity outcomes and pollution management in urban stormwater treatment wetlands. *Journal of Environmental Management, 233*, 302–307.

Huminicki, D. M., & Rimstidt, J. D. (2009). Iron oxyhydroxide coating of pyrite for acid mine drainage control. *Applied Geochemistry, 24*(9), 1626–1634.

Kim, M. J., Nriagu, J., & Haack, S. (2002). Arsenic species and chemistry in groundwater of southeast Michigan. *Environmental Pollution, 120*(2), 379–390.

Koski, R. A., Munk, L., Foster, A. L., Shanks III, W. C., & Stillings, L. L. (2008). Sulfide oxidation and distribution of metals near abandoned copper mines in coastal environments, Prince William Sound, Alaska, USA. *Applied Geochemistry, 23*(2), 227–254.

Mahoney, C., März, C., Buckman, J., Wagner, T., & Blanco-Velandia, V. O. (2019). Pyrite oxidation in shales: Implications for palaeo-redox proxies based on geochemical and SEM-EDX evidence. *Sedimentary Geology, 389*, 186–199.

Masuda, H., Shinoda, K., Okudaira, T., Takahashi, Y., & Noguchi, N. (2012). Chlorite—source of arsenic groundwater pollution in the Holocene aquifer of Bangladesh. *Geochemical Journal, 46*(5), 381–391.

Mehra, O. P., & Jackson, M. L. (2013). Iron oxide removal from soils and clays by a dithionite–citrate system buffered with sodium bicarbonate. *Clays and clay minerals* (pp. 317–327). Elsevier.

Mierzykowski, S. E., & Carr, K. C. (2000). *Trace element exposure in benthic invertebrates from grove Pond, plow shop Pond, and nonacoicus brook Ayer Massachusetts*. U.S. Fish and Wildlife Service, Maine Field Office.

Mohod, C. V., & Dhote, J. (2013). Review of heavy metals in drinking water and their effect on human health. *International Journal of Innovative Research in Science, Engineering and Technology, 2*(7), 2992–2996.

Nordstrom, D. K. (1982). Aqueous pyrite oxidation and the consequent formation of secondary iron minerals. In J. A. Kittrick, D. S. Fanning, & L. R. Hossner (Eds.), *Acid sulfate weathering*. Wiley.

Ozdilek, H. G. (2002). *Distribution and transport of copper and lead in the Blackstone River Massachusetts*. Worcester Polytechnic Institute.

Pakostova, E., Grail, B. M., & Johnson, D. B. (2017). Indirect oxidative bioleaching of a polymetallic black schist sulfide ore. *Minerals Engineering, 106*, 102–107.

Parnell, Jr, R. A. (1982). Weathering processes and pickeringite formation in a sulfidic schist: A consideration in acid precipitation neutralization studies. *Environmental Geology, 4*(3–4), 209–215.

Percak-Dennett, E., He, S., Converse, B., Konishi, H., Xu, H., Corcoran, A., Noguera, D., Chan, C., Bhattacharyya, A., Borch, T., & Boyd, E. (2017). Microbial acceleration of aerobic pyrite oxidation at circumneutral pH. *Geobiology, 15*(5), 690–703.

Perkins, R. B., & Mason, C. E. (2015). The relative mobility of trace elements from short-term weathering of a black shale. *Applied Geochemistry, 56*, 67–79.

Qiu, H., Gui, H., & Song, Q. (2018). Human health risk assessment of trace elements in shallow groundwater of the Linhuan coal-mining district, Northern Anhui Province, China. *Human and Ecological Risk Assessment: An International Journal, 24*(5), 1342–1351.

Richardson, J. B. (2020). Comparing trace elements (As, Cu, Ni, Pb, and Zn) in soils and surface waters among montane, upland watersheds and lowland, urban watersheds in New England, USA. *Water, 13*(1), 59.

Richardson, J. B., Aguirre, A. A., Buss, H. L., Toby O'Geen, A., Gu, X., Rempe, D. M., & Richter, D. D. B. (2018). Mercury sourcing and sequestration in weathering profiles at six critical zone observatories. *Global Biogeochemical Cycles, 32*(10), 1542–1555.

Richardson, J. B., Donaldson, E. C., Kaste, J. M., & Friedland, A. J. (2015). Forest floor lead, copper and zinc concentrations across the northeastern United States: Synthesizing spatial and temporal responses. *Science of the Total Environment, 505*, 851–859.

Richardson, J. B., Mischenko, I. C., Mackowiak, T. J., & Perdrial, N. (2022). Trace metals and metalloids and Ga/Al ratios in grey shale weathering profiles along a climate gradient and in batch reactors. *Geoderma, 405*, 115431.

Robinson, P., & Goldsmith, R. (1991). Stratigraphy of the Merrimack belt, central Massachusetts. *US Geological Survey Professional Paper, 1366,* G23–G37.

Robinson, P., Hollocher, K. T., Tracy, R. J., & Dietch, C .W. (1982). High grade Acadian regional metamorphism in south-central Massachusetts.

Roy, J. W., & Bickerton, G. (2010). Proactive screening approach for detecting groundwater contaminants along urban streams at the reach-scale. *Environmental Science & Technology, 44*(16), 6088–6094.

Santangelo, L. M., Brown, C. J., Shanley, J. B., Pribil, M. J., & Rutherford, D. L. (2022). Occurrence and sources of lead in private wells, Sturbridge Massachusetts. *Applied Geochemistry, 139*, 105231.

Sotiropoulos, J. C., Nislow, K. H., & Ross, M. R. (2006). Brook trout, Salvelinus fontinalis, microhabitat selection and diet under low summer stream flows. *Fisheries Management and Ecology, 13*(3), 149–155.

Tracy, R. J., & Robinson, P. (1988). Silicate-sulfide-oxide-fluid reactions in granulite-grade pelitic rocks, central Massachusetts. *American Journal of Science, 288*, 45–74.

Walsh, G. J. (2002). *Bedrock geology in the vicinity of the Leicester Well Site, Paxton, Massachusetts.* US Department of the Interior, US Geological Survey.

Xian, H., Zhu, J., Tan, W., Tang, H., Liu, P., Zhu, R., Liang, X., Wei, J., He, H., & Teng, H. H. (2019). The mechanism of defect induced hydroxylation on pyrite surfaces and implications for hydroxyl radical generation in prebiotic chemistry. *Geochimica et Cosmochimica Acta, 244*, 163–172.

Yellen, B., & Boutt, D.F. (2010). A reach-scale study of dam-induced hyporheic exchange: Controlling mechanisms and effects, Deerfield River, Massachusetts. In AGU fall meeting abstracts (pp. H31D-1031).

Yuretich, R., Leonard, W., & Pohanka, S. (1989). Hydrogeologic factors affecting acid neutralization in Cadwell creek watershed, west central Massachusetts. *Water Resources Research, 25*(4), 644–654.

Zen, E. A., Goldsmith, R., Ratcliffe, N. M., Robinson, P., Stanley, R. S., Hatch, N. L., Shride, A. F., Weed, E.G. A., & Wones, D. R. (1983). Bedrock geological map of Massachusetts. *US Geological Survey, 1*(250,000).

Zhu, W., Young, L. Y., Yee, N., Serfes, M., Rhine, E. D., & Reinfelder, J. R. (2008). Sulfide-driven arsenic mobilization from arsenopyrite and black shale pyrite. *Geochimica et Cosmochimica Acta, 72*(21), 5243–5250.